Graph Spectral Analysis using Electroencephalography in Alzheimer Disease and Frontotemporal Dementia Patients

María Paula Bonomini[1,2], Eduardo Ghiglioni[1,3], and Noelia Belén Rios[1,3]

[1] Instituto Argentino de Matemática "Alberto P. Calderón" (IAM), CONICET, Argentina. paulabonomini@gmail.com
[2] Grupo Inteligencia Artificial - Universidad Tecnológica Nacional (UTN), Facultad Regional Haedo, Haedo, Bs. As., Argentina.
[3] Centro de Matemática La Plata (CMaLP) - Facultad de Cs. Exactas, Universidad de La Plata, Argentina.

Abstract. Graph theory has proven to be useful in studying brain dysfunction in Alzheimer's disease using magnetoencephalography (MEG) and fMRI signals. However, it has not yet been tested enough with reduced sets of electrodes, as in the 10-20 EEG. In this work, we applied techniques from the graph spectral analysis (GSA) derived from EEG signals of patients with Alzheimer, Frontotemporal Dementia and control subjects. A collection of global GSA metrics were computed, accounting for general properties of the adjacency or Laplacian matrices. Also, regional GSA metrics were calculated, disentangling centrality measures in five cortical regions (frontal, central, parietal, temporal and occipital). These two sort of measures were then utilized in a binary AD/controls classification problem to test their utility in AD diagnosis and identify most valuable parameters. The Theta band appeared as the most connected and synchronizable rhythm for all three groups. Also, it was the rhythm with most preserved connections among temporal electrodes, exhibiting the shortest average distances among T_3, T_4, T_5 and T_6. In addition, Theta emerged as the rhythm with the highest classification performances based on regional parameters according to a k=5 cross-validation scheme (mean accuracy=0.74±0.03, mean recall=0.72±0.05 and mean F1-score=0.72±0.03). In general, regional parameters produced better classification performances for most of the rhythms, encouraging further investigation into GSA parameters with refined spatial and functional specificity.

Graph Spectral Analysis EEG Alzheimer Disease

1 Introduction

Alzheimer's disease (AD) and Frontotemporal dementia (FTD) represent two distinct neurodegenerative disorders, each characterized by unique clinical manifestations and neuropathological profiles. AD is physiologically characterized by

the accumulation of amyloid-plaques and neurofibrillary tangles of tau protein in the brain, leading to neuronal death. AD symptoms consist mainly of memory loss and cognitive decline, which is largely due to damage in the hippocampus. The hippocampus is a brain structure, located in the medial temporal lobe (MTL), which plays a central role in the creation of new memories and the storage of existing memories. On the other side, FTD is more often characterized by early changes in behavior, personality, and language, depending on the variant. Even though Alzheimer's disease and frontotemporal dementia present overlapping features in advanced stages, early discrimination between them remains crucial due to their distinct clinical trajectories, management strategies, and prognoses. This clinical heterogeneity poses a challenge for differential diagnosis, particularly when relying solely on neuropsychological assessments. Recent advances in neuroimaging and electrophysiological techniques, such as EEG, have opened new possibilities for distinguishing between these conditions.
Machine learning and deep learning techniques have been widely used in AD detection for a long time. Examples can be found at [1, **?**,**?**,**?**]. In addition to AD classification, other reports employed decomposition methods in their studies. For example, Amezquita-Sanchez et al. introduced the Complete Ensemble Empirical Mode Decomposition with permutation entropy for detecting subjects with impaired working memory [2]. In other studies, multiple signal classification and empirical wavelet transform with nonlinear features such as fractal dimension were analyzed [3], or implemmentation of classification algorithms based on enhanced probabilistic neural network models [4, **?**].
The use of graph theory to study AD, however, is relatively new. One of the pioneering work is from Stam et al. [5], who investigated whether functional brain networks were abnormally organized in AD by EEG signals. In particular, he stated that healthy brains tended to present high clustering coefficients and low path lengths, which means that healthy networks have "small world" structure. In addition, the presence of small world structures tended to disappear in AD patients. Since then, several authors have used graph theory tools to study connectivity and the existence of different patterns in AD.
There is a large amount of information available in the literature regarding Alzheimer's Disease, Adeli et al. [6] provide an extensive review of research on computational modeling of AD and its markers. Their work covers neurological models, brain imaging analysis, EEG feature extraction, classification models, and neural models of memory. Additionally, Adeli et al. [7] offer another review focusing on time-frequency analysis, wavelet analysis, and chaos analysis. For a general overview of the clinical neurophysiology of AD, we recommend Bhat et al. [8]. In the same domain, Hulbert et al. [9] review studies related to EEG and MEG.

Despite their utility, graph representations lack standardization, which poses significant challenges when comparing the topology and organization of different networks [10]. Such comparisons often depend heavily on variables like network size or density. To address these limitations, Graph Spectral Analysis (GSA) has emerged within graph theory as a robust approach.

GSA focuses on analyzing the intrinsic properties of graphs by examining the spectral characteristics of their Adjacency or Laplacian matrices, providing a more universal framework for network evaluation. The advantage of GSA is to deduce invariant properties and structure of a graph from a list of spectral tools that are easily computable and play a central role in our fundamental understanding of graphs.
Late in 2012, de Haan et al. presented their first reports associating GSA and Alzheimer [11]. They studied the disruption of functional brain networks in AD by magnetoencephalography (MEG) signals. In particular, they focused on network connectivity, synchronizability and node centrality. The main outcomes from their work were a general loss of connectivity, altered synchronizability and depressed centrality in the temporal MEG channels.
EEG and MEG are two complementary, non-invasive neuroimaging techniques used in the diagnosis of various brain disorders. A key distinction lies in their cost and technical capabilities: EEG is more cost-effective, whereas MEG offers superior sensitivity and spatial resolution, a difference partly attributed to the greater number of channels available in MEG for signal acquisition.
Following de Haan ideas, we aimed at studying the possibilities of GSA in EEG 10-20 configurations, a setup greatly reduced with respect to MEG, in terms of number of channels and spatial resolution. The potential advantage of successfully applying GSA to EEG lies in its easy accessibility, low cost, clinical interpretation and short study durations that the technique offers.
In this study, we investigated whether global and regional GSA metrics derived from EEG recordings can effectively distinguish between control participants and AD/FTD patients. To achieve this, we analyzed network connectivity, node centrality, stabilization, and path-length distances to evaluate disruptions in functional brain networks. Also, we addressed a binary AD/control classification problem based on global and regional GSA metrics. These analyses align with Stamm's "small-world" simulations and De Haan's MEG findings, providing a comprehensive framework for understanding alterations in neural connectivity on the EEG recording modality.

2 Materials

2.1 Dataset Description

The data utilized in this study were sourced from the OpenNeuro repository (https://openneuro.org/), specifically the dataset identified as DS004504 [12]. This data set comprises electroencephalographic (EEG) recordings from individuals diagnosed with Alzheimer's disease (AD), frontotemporal dementia (FTD) and healthy controls of the same age.

The dataset includes a total of 88 participants, categorized into three groups: AD patients (n = 36), FTD patients (n = 23), and healthy controls (n = 29). Participants were matched for age and other demographic characteristics to reduce potential confounding variables. In fact, age appeared as an unbiased demographic parameter (AD: 66.38 ± 7.77 yo vs Controls: 67.89 ± 5.30 yo, p =

0.3829, Mann-Whitney test). However, gender did present a bias in the AD vs Control groups (AD: 24/35 women vs Controls: 11/30 women, p = 0.0394, $Chi - squared$ test). The clinical diagnoses of AD and FTD were determined according to established diagnostic criteria, incorporating comprehensive neuropsychological assessments and clinical evaluations conducted by experienced professionals. Cognitive and neuropsychological state was evaluated by the international Mini-Mental State Examination (MMSE). MMSE score ranges from 0 to 30, with lower MMSE indicating more severe cognitive decline. The average MMSE for the AD group was 17.75 (sd=4.5), for the FTD group was 22.17 (sd=8.22) and for the CN group was 30 (sd = 0). The duration of the disease was measured in months and the median value was 25 with IQR range (Q1-Q3) being 24 - 28.5 months. Concerning the AD groups, no dementia-related comorbidities have been reported.
Recordings were acquired from the 2nd Department of Neurology of AHEPA General Hospital of Thessaloniki by an experienced team of neurologists. For recording, a Nihon Kohden EEG 2100 clinical device was used, with 19 scalp electrodes (Fp1, Fp2, F7, F3, Fz, F4, F8, T3, C3, Cz, C4, T4, T5, P3, Pz, P4, T6, O1, and O2) according to the 10-20 international system and 2 reference electrodes (A1 and A2) placed on the mastoids. Each recording was performed with participants being in a sitting position having their eyes closed. The sampling rate was 500 Hz with 10uV/mm resolution.

3 Methodology

The EEG signals in the dataset underwent preprocessing and denoising using the Independent Component Analysis (ICA) method. Initially, a Butterworth band-pass filter (0.5–45 Hz) was applied to attenuate baseline drift and high-frequency noise. Subsequently, the signals from the 19 EEG channels were linearly decomposed into 19 independent components. Components identified as artifacts, specifically those associated with jaw or ocular activity, were excluded. The remaining components, representing artifact-free EEG activity, were used to reconstruct the original 19 EEG channels. Following ICA-based denoising, the signals were re-referenced to the A1-A2 montage.
On these signals, we have then accomplished rhythm selection on the following frequency bands: delta (0.5-4 Hz), theta (4-8 Hz), alpha (8-12 Hz), beta (12-30 Hz) and gamma (30-45 Hz). Finally, four epochs lasting 7 secs were randomly selected between "boundary" annotations from the database. For each subject, functional connectivity and GSA metrics were independently computed for each epoch. Results were then averaged among these 4 epochs.

3.1 Functional Connectivity

Functional connectivity was estimated from the rhythm-filtered EEG recordings using the Phase Locking Value (PLV), a widely used measure that quantifies

the temporal consistency of the phase difference between pairs of oscillatory signals, regardless of their amplitude [13, ?]. This metric is particularly robust to amplitude variations and allows the assessment of transient or sustained phase couplings across different frequency bands. For every EEG channel j,k, the instant phase $\phi_j(t)$ and $\phi_k(t)$ was obtained by applying the Hilbert transform to the signals. Based on these phases, PLV was computed as follows:

$$PLV_{j,k} = \frac{1}{N} \sum_{t=1}^{N} e^{i(\phi_j(t) - \phi_k(t))} \tag{1}$$

where N represents the number of samples in the analysis window, and $(\phi_j(t) - \phi_k(t))$ corresponds to the instantaneous phase difference between the signals. The PLV value ranges from 0 (no synchronization) to 1 (complete synchronization), indicating the degree of phase coupling between the channels considered. The PLV values for each channel pair were organized into symmetric adjacency matrices A, where $A_{j,k} = PLV_{j,k}$. These matrices were interpreted as representations of functional networks, where nodes correspond to electrodes and weighted edges reflect the degree of phase synchronization between signal pairs.
The adjacency matrices were then thresholded at different levels, ranging from 05. to 0.9 in 0.1 increments. As a result, weighted thresholded matrices were obtained. We will call these matrices the Adjacency matrix $A(G)$ or simply A. In A, in turn, the degree matrix D was computed. D is a diagonal matrix that contains the total number of connections for every node (EEG channels). D's non-zero entries were computed by summing up the raws of the covariance matrix. Subsequently, the Laplacian L was calculated as the difference between D and A. The metrics presented in this work were calculated based on A and L. The analysis was systematically carried out for each threshold in order to assess the dynamics of the metrics in terms of the strength of connection.

3.2 Relative Power Spectral Density for rhythms

Finally, the relative power spectral density (PSD) was calculated for each band, by calculating each segment's squared magnitude of their discrete Fourier transforms. To obtain a relative PSD, the PSD of each rhythm was normalized as follows:

$$PSD_r(f) = \frac{\sum_{f_1}^{f_2} P(f)}{\sum_{f_l}^{f_h} P(f)} \tag{2}$$

where $[f_l, f_h] = [0.5,45]$ and $[f_1, f_2]$ are determined by the frequency ranges of the selected rhythm.

3.3 Graph theory tools for connectivity measures. Definitions and notation

In what follows we mention the definitions we need about graph theory. For more details see, for example, [14, 15]. Let G be a finite undirected weighted *graph*

without loops or multiple edges of n vertices labeled $1, 2, \ldots, n$. We denote the set of vertices of G by V (or $V(G)$). We say that two vertices i and j are *adjacent* (or neighbors) if they are joined by an edge and we write $i \sim j$. We denote the set of edges of G by E (or $E(G)$), where an edge ij belongs to E if and only if $i \sim j$. In this case, we say that the edge ij is *incident* with vertices i and j. The *degree* or *degree centrality* (DG) d_i of a vertex i is the number of edges incidents with it. We also denote by $N(i) := \{j : i \sim j\}$ the set of *neighbors* of the vertex i. G is a *weighted graph* if there exists a non-negative function $W_{ij} : V \times V \to \mathbb{R}$ such that $W_{ij} = W_{ji}$ and $W_{ij} > 0$ if $i \sim j$. Any weight W_{ij} induces a function on $V(G)$ given by

$$W(i) = \sum_{j \in N(i)} W_{ij} = \sum_{j \in V(G)} W_{ij}.$$

There exist three matrices associated to a (weighted) graph G in which we are particularly interested in: the *Adjacency matrix* $A \in \mathbb{R}^{n \times n}$ (or $A(G)$) given by $A_{ij} = W_{ij}$ if $ij \in E$ or 0 in another case; the *Degree matrix* $D \in \mathbb{R}^{n \times n}$ (or $D(G)$), which is a diagonal matrix with main diagonal given by the vector of (weighted) degrees $(W(1), \ldots, W(n))$; and the *Laplacian* $L = D - A$.
It is known that L is a symmetric and positive semi-definite matrix, then the eigenvalues of L are real and positive, so we denote by $\lambda_1 \leq \ldots \leq \lambda_n$ the eigenvalues of L counting multiplicities. Let $\mathbb{1} = (1, \ldots, 1) \in \mathbb{R}^n$, then $\mathbb{1}$ is an eigenvector of L associated to $\lambda_1 = 0$. The multiplicity of 0 states the number of connected components of G.
In this work, we studied the following spectral data given the Laplacian and the Adjacency matrix of a graph G:

- *Algebraic connectivity* (AC): It is the first non-null eigenvalue of L.
- *Laplacian energy* (LE): It is the the sum of the differences of each eigenvalue with respect to the mean eigenvalue:

$$LE(G) = \sum_{i=1}^{n} \left| \lambda_i - \frac{2m}{n} \right|.$$

- The *spectral gap* (SG) given by $\lambda_n - \lambda_{n-1}$ of L. It plays an important role in the distribution of energy (or information) of a system.
- *Eigenvector centrality* (EC). It measures the relevance of a node with respect to the importance of its neighbors, which gives a better picture of the highly connected regions (hub electrodes) [16, 17]. Note that A is a symmetric matrix whose entries are non-negative, so to calculate the EC we applied the Perron-Frobenius theorem, that is, if $\mu_1 \leq \ldots \leq \mu_n$ are the eigenvalues of A, then:
  - The *spectral radius* (SR) $\rho(A) := \max_{i=1,\ldots,n} |\mu_i|$ is an eigenvalue of A.
  - There exists an (unitary) eigenvector associated to the eigenvalue $\rho(A)$ such that every coordinate is no-negative.

If we call $x = (x_1, \ldots, x_n)$ to the unitary eigenvector associated to $\rho(A)$, then x_i denotes the centrality for the vertex i. So every node has a positive number

assigned that depends on the connection of the node. That is, a higher number corresponds to a node that is connected (indirectly) to many nodes.

Besides the spectral measures mentioned above, we also included some other metrics, detailed bellow:

The *clustering* coefficient C_i of a vertex i with degree d_i is usually defined as the ratio of the number of existing edges, denoted by e_i, between neighbors of i, and the maximum possible number of edges between neighbors if i. The formula for C_i is:

$$C_i = \frac{2e_i}{d_i(d_i - 1)}.$$

The clustering coefficient C ranges between 0 and 1. Usually C_i is averaged over all vertices to obtain a mean C of the graph (Global Clustering).

$$C = \frac{1}{n}\sum_{i=1}^{n} C_i.$$

The Global Clustering coefficient is an index of local structure. It is a ratio between all possible connections of a vertex and the collections that actually happens for that vertex. After calculating such a ratio per vertex, all ratios are then averaged.

Finally we use the *Dijkstra's algorithm* to calculate the length path between nodes corresponding to certain temporal brain cortex, specifically, we considered the path length between the nodes corresponding to $T_3 - T_4$ and $T_5 - T_6$.

3.4 Statistical Analysis

Data are presented as $mean \pm SD$. The analyses were performed separately for each epoch within a frequency band and a patient, then averaged out. Statistical significance was tested by the non-parametric Kruskal-Wallis test, useful for median comparison among two or more independent groups. Significance was considered for p-values < 0.05. When necessary, the Dunn test was performed applying Bonferroni as the p-adjustment for multiple comparisons. Finally, when comparing only AD and controls, the nonparametric Wilcoxon rank sum test was utilized.

To classify Alzheimer's disease (AD) patients and controls, an XGBoost classifier was implemented. Two different datasets were tested. A first one consisted of global features extracted from EEG graphs, such as AC, LE, SG, SR and Global Clustering coefficient. The second one used the regional parameters Eigenvector Centrality, Local Clustering and Degree Centrality grouped into five brain regions (frontal, central, temporal, parietal, and occipital). A 5-fold stratified cross-validation approach was applied to evaluate the model, ensuring a balanced representation of classes in each fold. The XGBoost classifier was trained with 300 estimators, a learning rate of 0.01, a maximum depth of tree of 5 and a subsample size of 0.7. It was evaluated using metrics such as precision, recall, and

F1 score, following a k-cross validation scheme with k=5. The cross-validation results provided mean and standard deviation values for each metric. The dataset was split into training (80%) and test (20%) subsets. Feature importance was calculated using the XGBoost model and the contribution of each EEG-derived feature to the classification was analyzed.

4 Results

4.1 Relative Power Spectral Density

The first exploratory analysis performed on the data was related to the relative Power Spectral Density (PSD_r) of each band. Figure 1 shows the PSD_r for every group and every rhythm. Notice that, consistently with the literature, AD patients presented a significant increase in PSD_r for theta and delta bands and a significant decrease in the alpha and beta bands (Kruskal-Wallis test with Dunn's post hoc analysis, $p < 0.016$, Bonferroni correction applied to post hoc comparisons), evidencing a shift toward low frequencies in this group [18].
In particular, the gamma band showed the lowest energy among all EEG frequency bands, an observation that may align with the fact that gamma rhythms are strongly associated with cognitive load, not elicited by this experimental task. In the opposite end, the delta band presented the highest PSD_r for all three groups, also in line with the literature [18].

4.2 GSA metrics

After rhythm selection, a thresholded adjacency matrix was conformed by PLV analysis. When inspecting the adjacency matrices at different thresholds, a greater loss in the functional connections of AD patients can be observed, especially in the temporal electrodes. Figure 2 shows the adjacency matrices, graph topologies and Eigenvector Centrality of a representative AD patient (a) and a control subject (b) in the theta band at three different thresholds. Notice that in both cases, graphs are fully connected for a threshold of 0.5, but from 0.7 on, there exists a greater loss of connections in the AD case. Furthermore, a decrease of connectivity in the temporal electrodes with threshold can be appreciated in the AD patient, as observed for thresholds 0.7 and 0.9. Moreover, the temporal T_6 electrode shows an early blackout at threshold 0.5 (Fig 2a, Th = 0.5). These measures are supported by the EC values across electrodes (middle panels). Fundamentally, at thresholds 0.7 and 0.9, a decrease in EC can be observed in the temporal region. In contrast, Controls kept the EC values more uniform across the electrodes, preserving to a greater extent the overall connectivity scheme.

The intuitive idea presented in Figure 2 was systematically analyzed for the three groups in Figure 3, where the network connectivity was quantified by Algebraic Connectivity (AC) and Laplacian Energy (LE) for different rhythms

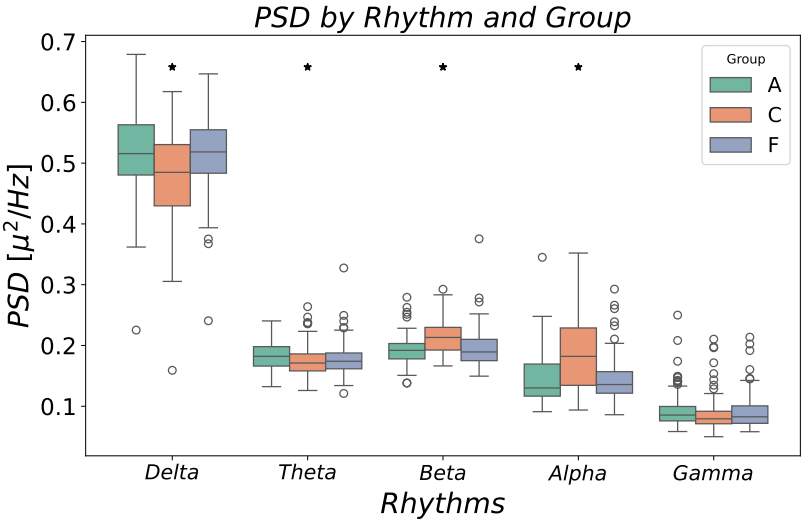

Fig. 1: Relative PSDs (PSD_r) across groups for the five rhythms analyzed. Notice that α and β rhythms resulted enhanced, while delta and theta depressed in the controls with respect to AD or FT groups. * : $p < 0.016$, (Kruskal-Wallis test with Dunn's post hoc analysis, Bonferroni correction applied to post hoc comparisons).

and thresholds. Control subjects presented greater AC values than Alzheimer or Frontotemporal patients for all thresholds in the theta and delta bands (Kruskal-Wallis test with Dunn's post hoc analysis, $p < 0.016$, Bonferroni correction for post hoc comparisons), while the trend was opposite for the beta and alpha bands (p = NS), with very little connectivity in the gamma band (p = NS). Please note that the delta band was not shown for spatial organization of the graphics, but it followed the theta pattern in terms of trend and statistical significance. Despite showing different patterns across rhythms, it is evident that controls presented the least loss of connections as threshold increased, either for the case where they had greater or lower number of connections at low thresholds. In fact, initially lower AC values for controls ended up matching those of AD or FT patients at thresholds 0.8 and 0.9. In addition, theta was the rhythm accounting for the most of AC regardless the group, presenting much lower AC values for the remaining bands.

In particular in patients with AD, the highest overall connectivity was shown for the theta band, although significantly lower than the controls, and decreased its connectivity levels for the remaining bands, showing no significant differences with respect to controls. This is consistent with the reported shift of AD operation towards slower rhythms, such as the theta and delta band [18]. Finally, the

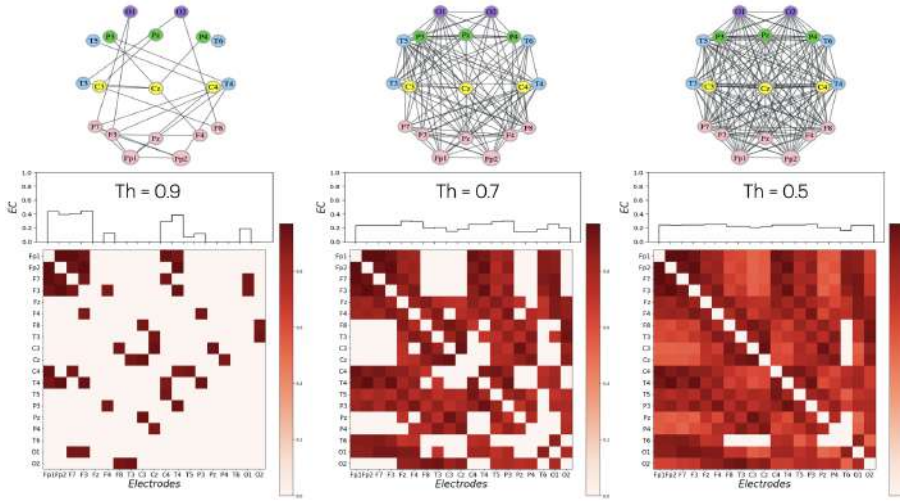

(a) Alzheimer patient

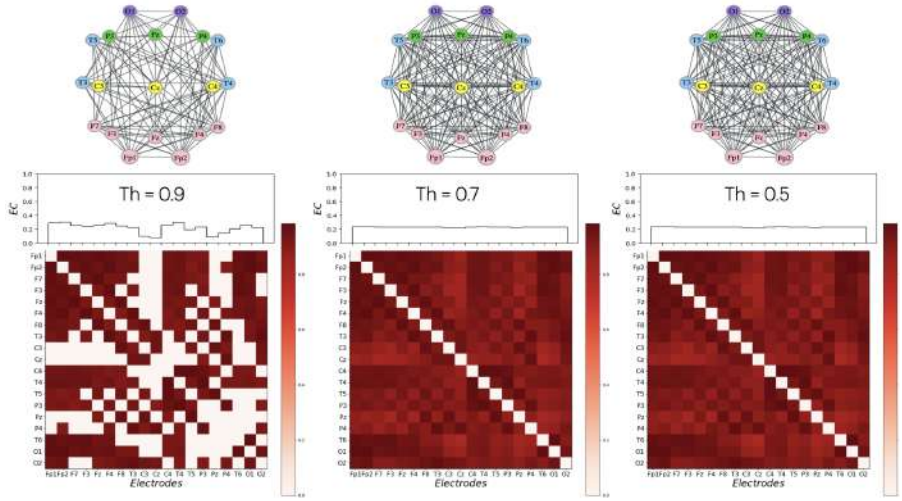

(b) Control patient

Fig. 2: Functional connectivity versus threshold. Adjacency matrices (lower panel), graphs topologies (upper panel) and Eigenvector Centrality values (middle panel) of a representative AD patient (a) and a control subject (b), both in the theta band at three different thresholds (th = 0.9, 0.7, 0.5).

band with the lowest AC values for controls, FT or AD patients was the gamma band. This fact is consistent with the nature of the task and the relative PSD of the band (see Fig. 1).

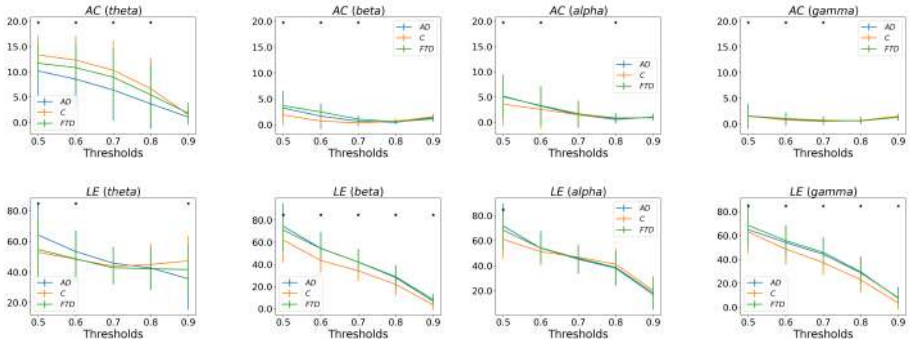

Fig. 3: Algebraic connectivity (AC) and Laplacian Energy (LE) error-bars for every rhythm and threshold. Notice the inverse relationship between AC and LE. * : $p < 0.016$, (Kruskal-Wallis test with Dunn's post hoc analysis, Bonferroni correction applied to post hoc comparisons).

In opposition to AC, Laplacian energy (LE) showed consistent patterns across rhythms and thresholds. In fact, LE turned out to be significantly lower for controls than AD or FT patients in most frequency bands and thresholds. The fact that controls presented low LE values can be interpreted in terms of diffusion in a network. That is, the lower the LE, the faster a perturbation or information spreads through the net, which implicitly leads to the idea of a more homogeneous network.

When assessing the relative importance of a node within a network, on the other hand, a bunch of graph measures come up [19]. The most straightforward metric is the *Degree Centrality*, which assigns a hub status to nodes according to its number of connections. Alternative measures focus on the concept of centrality, with betweenness or closeness centrality as examples, with some problems related to computational demands [20]. *Eigenvector Centrality*, on the other hand, takes into account both the degree of a node and the degrees of its neighbors [21]. In Fig. 4 we compare three metrics for node centrality assessment on a cortical region basis. On the left panel, the *Degree Centrality* is displayed, in the middle panel the *Eigenvector Centrality* can be seen, and on the rightmost panel the *Local Clustering*, all of them disentangled for specific brain regions. In this case, we have grouped electrodes into 5 different cortical regions, namely: frontal electrodes (F), central electrodes (C), temporal electrodes (T), parietal electrodes (P) and occipital electrodes (O). All five regions have been computed for all frequency bands at threshold 0.9. Notice that AD patients showed a diminished *Degree Centrality* for the Delta and Theta bands ($p < 0.016$, Kruskal-Wallis), whereas remained similar to other groups in the Beta, Alpha and Gamma groups, with much lower values. The same behavior was evidenced for *Local Clustering* on a brain region basis. In both cases, an AD decrease in the temporal and frontal regions can be appreciated for both metrics in all bands. Moreover, an alternating pattern can be found around frontal, cen-

tral and temporal electrodes in *Eigenvector Centrality* and *Local Clustering* at Beta, Alpha and Gamma frequency bands.

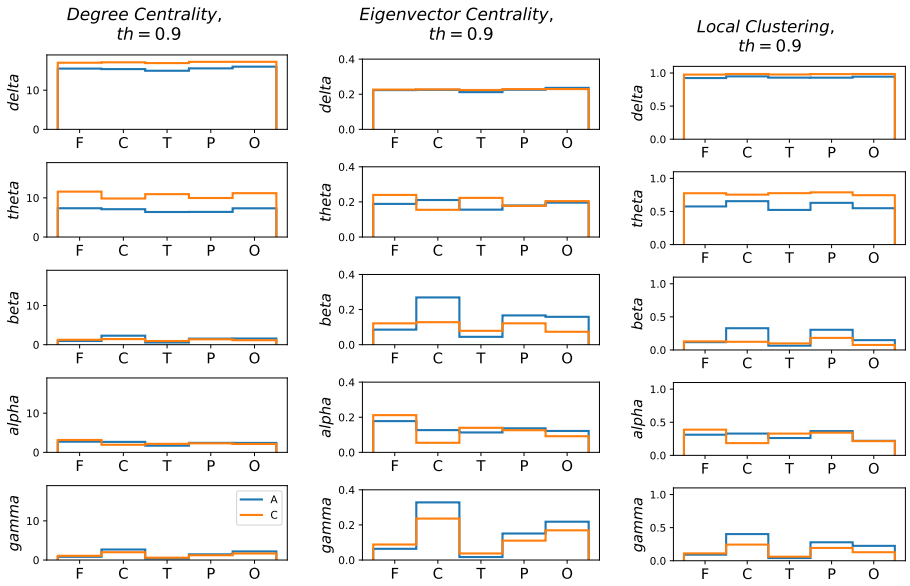

Fig. 4: Centrality metrics comparison. Degree centrality, Eigenvector centrality (EC) and Local Clustering were calculated for all frequency bands at threshold 0.9, and every cortical region, namely, F: frontal, C: central, T: temporal, P: parietal and O: occipital. Blue: Alzheimer group, Red: Controls. Notice that lower rhythms (Delta, Theta) accounted for most of the network centrality.

We can see in Fig. 5, an analysis of the path length across electrodes in the temporal cortical region for every rhythm and threshold. In the upper panels, the global clustering coefficients are displayed, in conjunction with an average *Dijkstra* path length from two pairs of temporal electrodes $T_3 - T_4$ and $T_5 - T_6$ (middle panel). Since path length between electrodes can be poorly standardized due to disconnected electrodes, the disconnection rate of these temporal electrodes is also included on the bottom panel. Notice that Theta came up as the rhythm with minimum disconnection rate (50 % maximum for AD group, 25% for C or FT groups) for all three groups, particularly for controls, for whom they showed the shortest path length among temporal electrodes. For the remaining rhythms, disconnection rates of temporal electrodes achieved 80 %, presenting much longer path distances. These minimum path lengths for the Theta rhythm, in turn, were accompanied by the highest *Global Clustering* co-

efficients, which resembles the concept of small world defined by Stamm et al. [5].

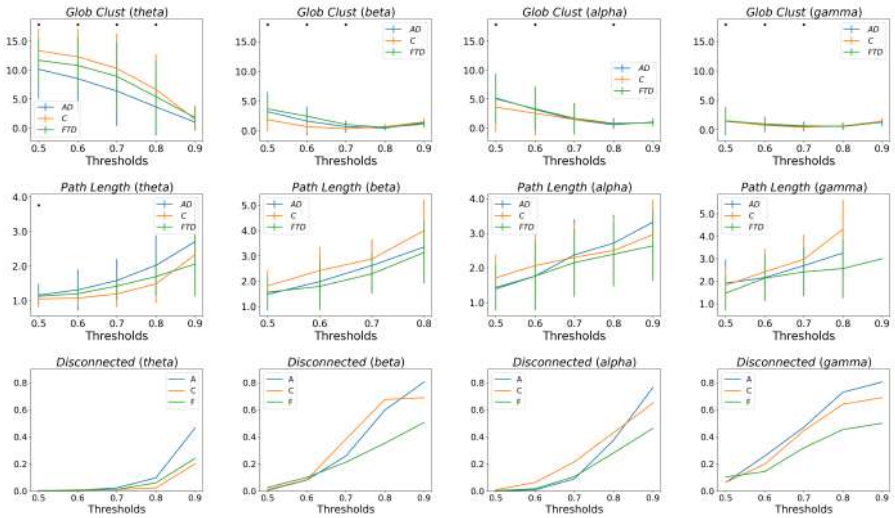

Fig. 5: Path length and Disconnection rate across temporal electrodes. Middle) Errorbars for Average path length between the pairs of temporal electrodes T_3-T_4 and T_5-T_6. Bottom) Disconnected channels for every rhythm and threshold. Top) Overall Global Cluster coefficients for the entire network. * : $p < 0.016$, (Kruskal-Wallis test with Dunn's post hoc analysis, Bonferroni correction applied to post hoc comparisons).

From this figure, we can see that Global Clustering follows AC (see Fig. 3), at least in terms of trends. In addition, we can infer an inverse relationship between density and the average length of the path among the temporal electrodes, measured by the *Dijkstra* algorithm. This makes sense, since the higher the amount of connections (on average) in a graph, the more likely the graph is uniformly connected. This combination of a high number of connections and short paths resembles, at least conceptually, the *small worlds*, considered recently by Stam [22]. Note that Beta and Gamma produced the highest amount of disconnected electrodes, followed by Alpha. Consistently, the theta band produced the lowest disconnection rates, accordingly with the lowest mean distances for every group, highest Global Clustering levels and AC values (see Fig. 3).
To complete the set of SGA tools, we also computed the Spectral Gap (SG) and Spectral Radius (SR). SG values tell about how long the functional network dynamics take to reach a stable state. Thus, a small SG means a fast adaptation to perturbations. In the theta band, Controls presented a faster synchronizability at thresholds 0.5, 0.6, 0.7 and 0.8, since they exhibited significantly decreased SG values (Kruskal-Wallis test with Dunn's post hoc analysis, $p < 0.016$, Bon-

ferroni correction for post hoc comparisons). The same trend, although not at the corrected significance levels, was found for the alpha and delta bands. This observation aligns with the physical interpretation of SG. This is, if a physical system was modeled as a graph, a small spectral gap indicates that the network allows information to flow more easily through it, while a large spectral gap suggests greater resistance to dispersion [23]. In this case, controls would resist the less information flow, or, in other words, AD neuronal networks would conform more rigid systems. It is worth noting that this physical interpretation coincides with that from the Laplacian Energy, presenting quite consistent results.
The Spectral Radius, meanwhile, reflects the interconnectivity of a network. The higher the SR, the more dense the network. With respect to SR, the beta and theta bands made the difference. Table 1 shows the mean ± SD SR values for rhythm and threshold throughout groups. Bold numbers denote statistical significance at a Bonferroni adjusted p-value of 0.016. In the theta band, the A group was significantly lower than the controls, while no difference was reported for the F group. However, the beta band showed significantly lower SR values for controls against the A or F groups. However, when analyzing the AD group against itself for all thresholds, we can see that the maximum SR value on average was present in the theta band, suggesting that AD neuronal networks operate mainly in this frequency band.

EEG		**Threshold**				
Rhythm		**0.5**	**0.6**	**0.7**	**0.8**	**0.9**
Delta	A	**16.99** ± 2.43	**16.96** ± 2.90	**16.89** ± 2.82	**16.65** ± 2.08	**15.76** ± 1.14
	C	**17.43** ± 2.95	**17.42** ± 3.02	**17.40** ± 2.87	**17.37** ± 2.39	**17.15** ± 1.21
	F	**16.77** ± 3.31	**16.73** ± 3.62	**16.59** ± 3.69	**16.29** ± 2.54	**15.20** ± 1.34
Beta	A	**10.74** ± 2.43	**9.35** ± 2.90	**7.26** ± 2.82	**4.83** ± 2.08	**2.39** ± 1.14
	C	**8.49** ± 2.95	**7.08** ± 3.02	**5.39** ± 2.87	**3.72** ± 2.39	**1.69** ± 1.21
	F	10.62 ± 3.31	**9.56** ± 3.62	**7.65** ± 3.69	**5.10** ± 2.54	2.42 ± 1.34
Theta	A	**13.65** ± 2.70	**12.95** ± 3.28	**11.92** ± 3.83	**10.03** ± 4.38	**6.83** ± 4.31
	C	**15.64** ± 1.40	**15.43** ± 1.79	**14.95** ± 2.42	**13.70** ± 3.52	**10.00** ± 4.59
	F	14.39 ± 2.94	13.95 ± 3.44	13.24 ± 4.09	12.06 ± 4.74	8.54 ± 4.74
Alpha	A	10.34 ± 2.93	9.23 ± 3.15	7.69 ± 3.092	5.49 ± 2.67	2.94 ± 1.68
	C	9.15 ± 3.41	8.49 ± 3.36	7.42 ± 3.05	5.84 ± 2.39	3.07 ± 1.33
	F	10.29 ± 3.17	9.28 ± 3.43	7.79 ± 3.59	5.70 ± 3.15	2.87 ± 1.83
Gamma	A	8.39 ± 2.67	7.42 ± 2.69	6.22 ± 2.41	4.56 ± 1.90	2.38 ± 1.20
	C	8.41 ± 2.62	7.32 ± 2.69	5.85 ± 2.66	4.35 ± 2.67	2.34 ± 2.51
	F	8.87 ± 2.46	7.87 ± 2.43	6.42 ± 2.06	4.61 ± 1.53	2.44 ± 1.23

Table 1: Network integration. Spectral Radius across threshold, group and EEG rhythm.

4.3 Classification between AD patients and controls

In order to answer the question addressed in this work related to the utility of GSA for AD diagnosis in EEG records, we attempted to run some simple AI models to assess the performance of these GSA metrics when used in the binary AD/Controls classification problem. As usual, before jumping into an AI model, an exploratory data analysis is desirable. Fig. 6 shows the kernel density estimates (KDEs) for almost every parameter analyzed in this work. KDEs for every rhythm and parameter were calculated on the entire population at a fixed threshold of 0.5 (middle panel). Parameters are aligned between the PSD scalp topology for a control subject (top) and an Alzheimer patient (bottom). Notice the decreasing power, evident on the scalp topologies, for higher rhythms in the AD patient, unlike the control subject. KDEs are refined histograms that tell about the parameter's probability distributions for every group, giving insight into their utility as markers for the diagnosis based on EEG of Alzheimer's disease. Note that either for the most connected or the least connected rhythms, Delta and Gamma, parameters tended to distribute normally, whereas in the remaining rhythms parameters showed more irregular distributions. In particular, the Alpha band exhibited bimodal distributions in many cases, such as SR, Global Clustering and AC.

Moving further into the classification problem, two different models have been trained in order to discern AD from controls; one using global parameters and the other one using regional parameters. Table 2 shows the performances for an XGBoost binary classification under a cross validation scheme (k=5), by rhythm and modality (global vs regional parameters). In addition to the GSA features, age was included in all cases. It can be appreciated a better performance of the regional parameters over the global ones for most rhythms. Theta appeared as the rhythm with the best metrics for both the global and the regional parameters.
The three most important features, on the other hand, are presented in Table 2 for each modality. Note that the global feature EC_{av} ranked top-3 in all of the outputs, whereas EC_C and age appeared as the most important parameters in the regional case. Moreover, the model for the Theta band in the regional modality exhibited 2 out of 3 top-3 features (the eigenvector and degree centralities) associated to the temporal cortical region. Supporting this observation, Fig 7 displays the Receiver Operating Characteristic (ROC) curves for both modalities: Global features (left) and Regional features (right) for every rhythm at threshold 0.7. Note the superiority of the area under the curve (AUC) values for regional features against global ones.

5 Discussion

The main contribution of this paper is the collection of evidence supporting the usefulness of GSA in EEG signals, using a reduced 10-20 setup, for distinguish-

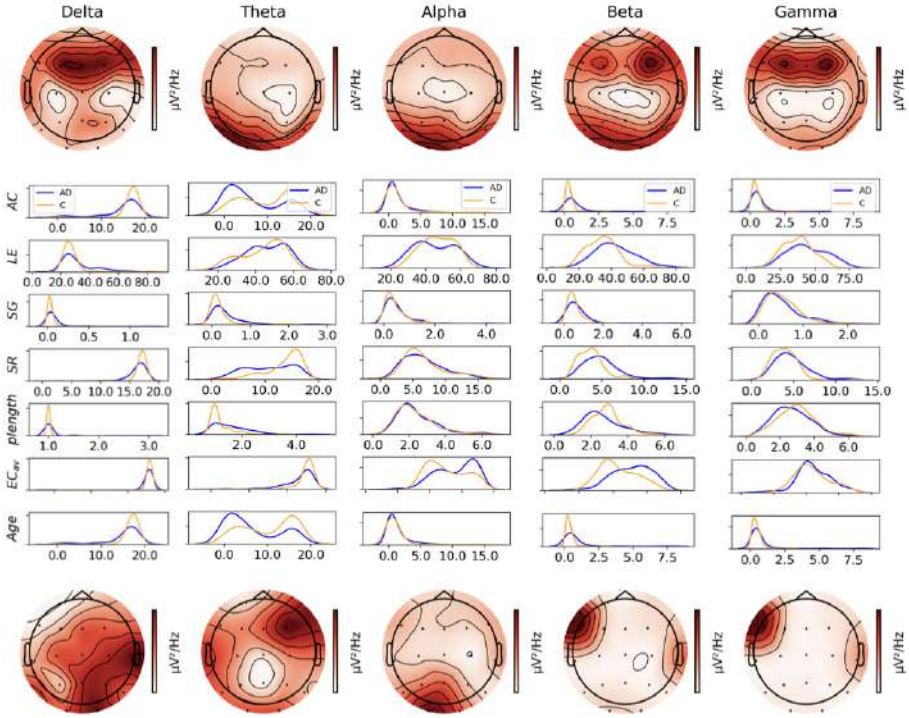

Fig. 6: Kernel density estimates (KDEs) and scalp PSD topologies. Middle) Parameters KDEs for threshold 0.7 across Alzheimer (blue) and Controls (red). Alzheimer distributions are far more distant to normal distributions than Controls are. Top) Scalp PSD topologies by rhythm for a representative Alzheimer patient. Note the energy decrease with rhythm's central frequencies. Bottom) Scalp PSD topologies for a Control subject.

EEG		**Metrics**			
Rhythm	**Mode**	**Accuracy**	**Recall**	**F1-score**	**Features**
Delta	Global	0.67 ± 0.06	0.70 ± 0.16	0.66 ± 0.09	SR, EC_{av}, AC
	Regional	$\mathbf{0.72} \pm 0.05$	$\mathbf{0.78} \pm 0.07$	$\mathbf{0.73} \pm 0.05$	DC_T, Age, DC_F
Beta	**Global**	$\mathbf{0.64} \pm 0.06$	$\mathbf{0.67} \pm 0.16$	$\mathbf{0.64} \pm 0.06$	SR, EC_{av}, $plength$
	Regional	0.64 ± 0.07	0.50 ± 0.10	0.57 ± 0.06	EC_C, DC_P, DC_C
Theta	**Global**	$\mathbf{0.76} \pm 0.08$	$\mathbf{0.78} \pm 0.04$	$\mathbf{0.76} \pm 0.03$	SG, EC_{av}
	Regional	$\mathbf{0.71} \pm 0.04$	$\mathbf{0.80} \pm 0.09$	$\mathbf{0.72} \pm 0.03$	EC_T, DC_T, EC_C
Alpha	Global	0.57 ± 0.07	0.60 ± 0.16	0.55 ± 0.12	EC_{av}, $plength$
	Regional	$\mathbf{0.67} \pm 0.09$	$\mathbf{0.71} \pm 0.14$	$\mathbf{0.67} \pm 0.10$	EC_C, EC_F, Age
Gamma	Global	0.66 ± 0.11	0.73 ± 0.25	0.67 ± 0.14	LE, EC_{av}, SG
	Regional	0.64 ± 0.03	0.75 ± 0.05	0.66 ± 0.02	EC_F, Age, DC_P

Table 2: Classification according to global or regional GSA parameters plus age. $Mean \pm std$ of accuracy, recall and F1-score for random forest model and a cross validation scheme with k=5, for an intermediate threshold = 0.7. EC_i: Eigenvector Centrality associated to i cortical region, DC_i: Degree Centrality associated to i cortical region. Notice that regional parameters that produced the best performance were associated to the temporal region: EC_T, DC_T.

ing Alzheimer patterns from controls. By successfully applying GSA to EEG, we highlight its advantages as a readily accessible, cost-effective, and time-efficient technique for brain network analysis.

Besides easy of access, GSA on small graphs has many advantages. Firstly, interpretability is increased. When dealing with fewer nodes, topological results (such as centrality or connectivity between specific regions) are easier to interpret clinically, especially if grouped by cortical regions (frontal, temporal, etc.). This is useful for linking functional biomarkers with specific clinical symptoms (e.g., loss of temporal connectivity in Alzheimer's). In fact, Table 2 and Figure 7 in the paper illustrate this, with regional GSA markers providing the best classification metrics and AUC values. Secondly, GSA metrics describe network connectivity in terms of their spectrum. The spectrum is invariant, since it depends only on the geometric structure of the graph and not on its graphical representation. This gives us an overview of the graph's connectivity, and also provides metrics, such as eigenvector centrality, that focus on local features within the network [23]. Finally, despite the reduced number of channels, the study shows that GSA with 10-20 EEG managed to identify significant differences between clinical groups (AD, FTD, controls), reproducing patterns similar to those observed in studies with MEG [22] or high-density EEG (e.g., loss of small-worlds, alteration in centrality, etc.) [11].

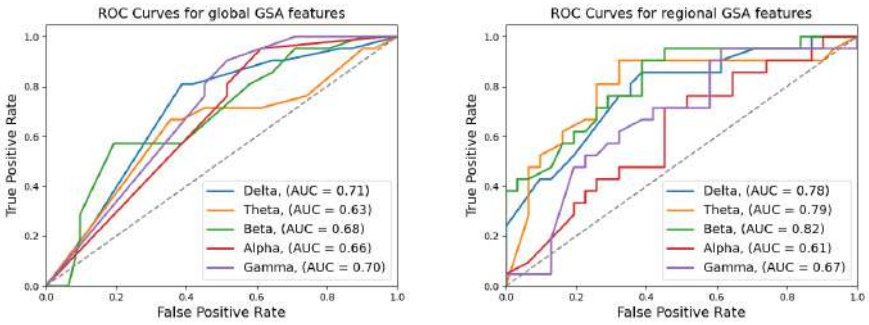

Fig. 7: Receiver Operating Characteristic (ROC) curves for global (left) and regional (right) parameters for all rhythms and threshold = 0.7. Note the superiority of regional features over global ones, producing the highest AUC values. AUC: Area under the curve.

Regarding distribution of energy across rhythms, our results confirmed the slowing down of EEG in AD patients, with powered theta and delta bands, and low alpha and beta bands (see Fig. 1), in consistency with the literature [18]. The predominance of theta as the strongest rhythm in AD patients, as revealed by relative PSD, aligns with the GSA findings—where theta and delta emerged as the preferred frequency bands displaying the highest connectivity, synchronizability, and dynamic properties in AD networks (see Figs. 3–5).

Using an increasingly higher threshold successfully revealed differences in connectivity between Alzheimer's disease (AD) patients and healthy controls, not only in the number of connections, but also in their strength (see Fig. 2). There is plenty of debate on graph thresholding. Techniques like proportional thresholding [24] or density-based thresholding [25] have been proposed, with the aim of standardizing the number of connections of graphs. These approaches force the graphs to contain the same number of connections, and therefore, same density, allowing comparison of graphs, eliminating density as a confounder [26]. However, the latter do not allow for the comparison of strength of connection and posses the drawback of including spurious connections if the rate of surviving connections or the desired density are badly selected. Maybe an hybrid thresholding approach might be adequate to test both topology and density simultaneously.

Network integration capacity of all three groups, reflected on the Algebraic Connectivity (AC) and the Density and the Spectral Radius (SR), was higher for controls in the Theta and Delta bands (see Fig. 3 and Table 1). At this point, a discrepancy with de Haan et al. [11] is found, since they reported significant AC changes in the beta, gamma and sub-alfa bands. In addition, their AC values differed considerably from those of this work, with very low values. We believe these differences are due to the following: First, the Adjacency matrix being constructed differently. We have utilized PLV followed by a thresholding procedure

whereas de Haan's used Synchronization Likelihood (SL) with no thresholding at all. In addition to SL [27], there are also other metrics for functional connectivity assessment, such as coherence analysis [28] or correlation coefficient [29]. In our experience, we compared LVP, coherence, and Pearson correlation coefficient, and LVP turned out to be the most cost-effective technique. While all three yielded similar results, LVP obtained the best performance from the XGboost model. Furthermore, coherence took excessively long to complete the analysis (4559 seconds), while LVP and Pearson correlation took 136 and 65 seconds, respectively. Second, DeHaan et al. analyzed MEG data, presenting higher spatial resolution, determined by 149 electrodes, unlike conventional EEG studies, which consist of twenty electrodes.

Regarding other functional connectivity measures, Mammone et al. [30] [31] employed a dissimilarity matrix, fundamentally differing from our PLV-based approach. In their method, the i,j-entry of the matrix represents a distance metric, specifically the Permutation Jaccard distance between elements i and j. By definition, this results in a matrix with zeros along the diagonal (since d[i,i]=0) and strictly positive off-diagonal values (as d[i,j]¿ for i $\neq$ j). In contrast, our framework utilizes a matrix derived from the difference of phase between pairs of EEG channels. Unlike a distance matrix, the adjacency matrix derived from PLV is not constrained by metric axioms; then, it does not require non-negativity or the triangle inequality. This distinction is evident in Fig. 2 (threshold = 0.9), where the graph associated to the adjacency matrix remains disconnected, while the dissimilarity matrix (due to its inherent distance properties) would always produce a connected graph. Thus, our approach offers greater generality, as it accommodates a broader spectrum of structural relationships. The adjacency matrix inherently captures both direct and indirect associations between channels, ensuring connectivity even under sparsity, whereas strict distance-based matrices may fail to preserve such global coherence.

Network integration, measured by the length of paths between nodes, was restricted in this study to the temporal cortical region. In this area, activity in the Theta band showed once again behavior compatible with a "small-world" organization, characterized by a high simultaneous capacity for integration and segregation [5]. This was reflected in high clustering coefficients and short average path lengths in the temporal region. This observation is consistent with that reported by Vecchio et al., who found significant differences in the characteristic path length and clustering coefficients of fMRI data in the Theta band from a global perspective [32]. Likewise, De Haan et al. reported a decrease in eigenvector centrality in the temporal region, accompanied by an increase in parietal areas, suggesting a compensatory functional reorganization [11]. In line with these findings, our results also revealed an increase in the centrality of parietal areas, along with a relative preservation or decrease in connectivity in temporal regions, which could be interpreted as a compensatory mechanism for the loss of efficiency in temporal regions.

Centrality measures, such as Eigenvector Centrality or the Global Clustering Coefficient, provide information about the network's segregation capacity. In

functional terms, segregation refers to the brain's ability to perform specialized processing within densely interconnected groups of cortical regions. In our analysis, the control group showed higher global clustering values in the Delta and Theta bands (see Fig. 4). Regarding local clustering, it was reduced in frontal and temporal electrodes for the Alzheimer's disease (AD) group, while controls showed a more uniform distribution across cortical regions. Although decreased temporal centrality in AD patients has been widely reported in the literature [21], frontal involvement has not been described with the same frequency , at least to our current knowledge.

One of the key contributions of this study is having demonstrated, that the loss of "small-world" organization observed in AD patients is closely linked to the decreased eigenvector centrality in two key cortical regions: the temporal and the frontal. Finally, regional rather than global parameters accomplished good performances in a binary classification task, with numbers comparable to the literature [33, **?**,**?**]. However, it should be mentioned that the classification in this study was only intended to compare the value of the global vs. regional GSA characteristics, but not to optimize an automated diagnosis of Alzheimer's.

6 Conclusions

This study highlights the potential of Graph Spectral Analysis (GSA) applied to 10-20 EEG recordings to identify distinctive patterns in Alzheimer's patients compared to healthy controls. Through global and regional metrics, our results suggest that theta and delta bands represent the most preserved rhythms in terms of connectivity and synchronization in Alzheimer's patients, whereas alpha and beta bands show a significant impairment. This finding supports the notion of a shift towards low frequencies in neural networks affected by Alzheimer's disease.

Network integration metrics, such as algebraic connectivity (AC) and spectral radius (SR), indicated a more robust network in healthy controls, particularly in theta and delta bands. On the other hand, centrality and segregation metrics, such as eigenvector centrality (EC) and clustering coefficient, showed significant alterations in temporal and frontal regions in Alzheimer's patients, underlining a weakening of the "small world" structures that characterize a healthy brain.

Additionally, this work provides evidence that GSA-derived parameters can be useful for binary classification problems (Alzheimer/Control), achieving an average accuracy of 71% in regional metrics for the theta band. These results not only highlight the applicability of GSA in more accessible and low-cost EEG contexts, but also open new opportunities for its use in diagnostics and longitudinal studies of neurodegenerative diseases.

In conclusion, this study validates the efficacy of GSA as a tool for the analysis of functional networks in the brain and lays the foundation for future research seeking to refine its diagnostic capacity and explore its applicability in clinical settings.

7 Acknowledgements

This work was (partially) supported by Programa Iberoamericano de Ciencia y Tecnología para el Desarrollo (CYTED) (through Red 225RT0169) and by CONICET (through PIP 11220210100954CO) .

References

1. G. Mirzaei and H. Adeli, "Machine learning techniques for diagnosis of alzheimer disease, mild cognitive disorder, and other types of dementia," *Biomed. Signal Process. Control.*, vol. 72, p. 103293, 2022.
2. J. P. Amezquita-Sanchez, A. Adeli, and H. Adeli, "A new methodology for automated diagnosis of mild cognitive impairment (mci) using magnetoencephalography (meg)," *Behavioural Brain Research*, vol. 305, pp. 174–180, 2016.
3. J. P. Amezquita-Sanchez, N. Mammone, F. C. Morabito, and H. Adeli, "A new dispersion entropy and fuzzy logic system methodology for automated classification of dementia stages using electroencephalograms," *Clinical Neurology and Neurosurgery*, vol. 201, 2020.
4. M. Ahmadlou and H. Adeli, "Enhanced probabilistic neural network with local decision circles: A robust classifier," *Integrated Computer-Aided Engineering*, vol. 17, no. 3, pp. 197–210, 2010.
5. C. J. Stam, B. F. Jones, G. Nolte, M. Breakspear, and P. Scheltens, "Small-world networks and functional connectivity in alzheimer's disease," *Cerebral Cortex*, vol. 17, no. 1, pp. 92–99, Jan 2007.
6. H. Adeli, S. Ghosh-Dastidar, and N. Dadmehr, "Alzheimer's disease and models of computation: imaging, classification, and neural models." *Journal of Alzheimer's disease : JAD*, vol. 7 3, pp. 187–99; discussion 255–62, 2005.
7. ——, "Alzheimer's disease: Models of computation and analysis of eegs," *Clinical EEG and Neuroscience*, vol. 36, pp. 131 – 140, 2005.
8. S. Bhat, U. R. Acharya, N. Dadmehr, and H. Adeli, "Clinical neurophysiological and automated eeg-based diagnosis of the alzheimer's disease," *European Neurology*, vol. 74, pp. 202 – 210, 2015.
9. S. Hulbert and H. Adeli, "Eeg/meg- and imaging-based diagnosis of alzheimer's disease," in *Reviews in the Neurosciences*, 2013.
10. B. C. Van Wijk, C. J. Stam, and A. Daffertshofer, "Comparing brain networks of different size and connectivity density using graph theory," *PloS one*, vol. 5, no. 10, p. e13701, 2010.
11. W. de Haan, W. M. van der Flier, H. Wang, P. V. Mieghem, P. Scheltens, and C. J. Stam, "Disruption of functional brain networks in alzheimer's disease: What can we learn from graph spectral analysis of resting-state magnetoencephalography?" *Brain connectivity*, vol. 2 2, pp. 45–55, 2012. [Online]. Available: https://api.semanticscholar.org/CorpusID:15428536
12. A. Miltiadous, K. Tzimourta, T. Afrantou, P. Ioannidis, and et. al, ""a dataset of eeg recordings from: Alzheimer's disease, frontotemporal dementia and healthy subjects"," 2024.
13. J.-P. Lachaux, E. Rodriguez, J. Martinerie, and F. J. Varela, "Measuring phase synchrony in brain signals," *Human Brain Mapping*, vol. 8, no. 4, pp. 194–208, 1999.

14. Z. Stanić, *Inequalities for graph eigenvalues*. Cambridge University Press, 2015, vol. 423.
15. P. Van Mieghem, *Graph spectra for complex networks*. Cambridge university press, 2023.
16. P. Bonacich, "Some unique properties of eigenvector centrality," *Soc. Networks*, vol. 29, pp. 555–564, 2007.
17. G. Lohmann, D. S. Margulies, A. Horstmann, B. Pleger, J. Lepsien, D. Goldhahn, H. Schloegl, M. Stumvoll, A. Villringer, and R. Turner, "Eigenvector centrality mapping for analyzing connectivity patterns in fmri data of the human brain," *PloS one*, vol. 5, no. 4, p. e10232, 2010.
18. R. Wang, J. Wang, H. Yu, X. Wei, C. Yang, and B. Deng, "Power spectral density and coherence analysis of alzheimer's eeg," *Cognitive Neurodynamics*, vol. 9, no. 3, pp. 291–304, June 2015.
19. S. Oldham, B. Fulcher, L. Parkes, A. Arnatkevic Iūtė, C. Suo, and A. Fornito, "Consistency and differences between centrality measures across distinct classes of networks," *PLoS ONE*, vol. 14, no. 7, p. e0220061, 2019. [Online]. Available: https://journals.plos.org/plosone/article?id=10.1371/journal.pone.0220061
20. M. Rubinov and O. Sporns, "Weight-conserving characterization of complex functional brain networks," *NeuroImage*, vol. 56, no. 4, pp. 2068–2079, Jun 2011, epub 2011 Apr 1. [Online]. Available: https://doi.org/10.1016/j.neuroimage.2011.03.069
21. L. Lorenzini, S. Ingala, L. E. Collij, V. Wottschel, S. Haller, K. Blennow, G. Frisoni, G. Chételat, P. Payoux, P. Lage-Martinez, M. Ewers, A. Waldman, J. Wardlaw, C. Ritchie, J. D. Gispert, H. J. M. M. Mutsaerts, P. J. Visser, P. Scheltens, B. Tijms, F. Barkhof, and A. M. Wink, "Eigenvector centrality dynamics are related to alzheimer's disease pathological changes in non-demented individuals," *Brain Communications*, vol. 5, no. 3, p. fcad088, Mar 2023.
22. C. J. Stam, W. De Haan, A. Daffertshofer, B. Jones, I. Manshanden, A.-M. van Cappellen van Walsum, T. Montez, J. Verbunt, J. C. De Munck, B. W. Van Dijk *et al.*, "Graph theoretical analysis of magnetoencephalographic functional connectivity in alzheimer's disease," *Brain*, vol. 132, no. 1, pp. 213–224, 2009.
23. F. R. K. Chung, *Spectral Graph Theory*, ser. CBMS Regional Conference Series in Mathematics. Providence, RI, USA: American Mathematical Society, 1997, vol. 92.
24. M. P. van den Heuvel, S. C. de Lange, A. Zalesky, C. Seguin, B. T. T. Yeo, and R. Schmidt, "Proportional thresholding in resting-state fmri functional connectivity networks and consequences for patient-control connectome studies: Issues and recommendations," *NeuroImage*, vol. 152, pp. 437–449, 2017.
25. A. Guénoche, "Clustering by vertex density in a graph," in *Classification, Clustering, and Data Mining Applications*, ser. Studies in Classification, Data Analysis, and Knowledge Organisation, D. Banks, F. R. McMorris, P. Arabie, and W. Gaul, Eds. Berlin, Heidelberg: Springer, 2004, pp. 15–23.
26. T. Adamovich, I. Zakharov, A. Tabueva, and S. Malykh, "The thresholding problem and variability in the eeg graph network parameters," *Scientific Reports*, vol. 12, no. 1, p. 18659, 2022. [Online]. Available: https://doi.org/10.1038/s41598-022-22079-2
27. C. J. Stam and B. W. van Dijk, "Synchronization likelihood: an unbiased measure of generalized synchronization in multivariate data sets," *Physica D: Nonlinear Phenomena*, vol. 163, no. 3-4, pp. 236–251, 2002.
28. M. Bonomini, M. Calvo, A. Morcillo, F. Segovia, J. Vicente, and E. Fernandez-Jover, "The effect of breath pacing on task switching and working memory." *Int J Neural Syst.*, vol. 30, p. 2050028, 2020.

29. B. d. C. M. Ordóñez, D. V. O. Villavicencio, M. A. S. Ochoa, and M. P. Bonomini, "Application of graph fourier transform in the diagnosis of left bundle branch block from electrocardiographic signals," in *Bioinspired Systems for Translational Applications: From Robotics to Social Engineering*, J. M. Ferrández Vicente, M. Val Calvo, and H. Adeli, Eds. Cham: Springer Nature Switzerland, 2024, pp. 495–503.
30. N. Mammone, C. Ieracitano, H. Adeli, A. Bramanti, and F. C. Morabito, "Permutation jaccard distance-based hierarchical clustering to estimate eeg network density modifications in mci subjects," *IEEE Transactions on Neural Networks and Learning Systems*, vol. 29, pp. 5122–5135, 2018.
31. N. Mammone, S. D. Salvo, L. Bonanno, C. Ieracitano, S. Marino, A. Marra, A. Bramanti, and F. C. Morabito, "Brain network analysis of compressive sensed high-density eeg signals in ad and mci subjects," *IEEE Transactions on Industrial Informatics*, vol. 15, pp. 527–536, 2019.
32. F. Vecchio, F. Miraglia, C. Marra, D. Quaranta, M. G. Vita, P. Bramanti, and P. M. Rossini, "Human brain networks in cognitive decline: a graph theoretical analysis of cortical connectivity from eeg data," *Journal of Alzheimer's Disease*, vol. 41, no. 1, pp. 113–127, 2014.
33. D. Klepl, F. He, M. Wu, D. J. Blackburn, and P. Sarrigiannis, "Eeg-based graph neural network classification of alzheimer's disease: An empirical evaluation of functional connectivity methods," *IEEE Transactions on Neural Systems and Rehabilitation Engineering*, vol. 30, pp. 2651–2660, Sep 2022.